International Symposium
On Turbulence and Shear Flow
Phenomena (TSFP-9)
June 30 - July 3, 2015 *Melbourne, Australia*

SCALAR DISPERSION BY COHERENT STRUCTURES

Christina Vanderwel
Department of Mechanical Engineering
University of Ottawa, Canada
(Current address: Aerodynamics and Flight Mechanics Research Group,
University of Southampton, United Kingdom)
c.m.vanderwel@soton.ac.uk

Stavros Tavoularis
Department of Mechanical Engineering
University of Ottawa, Canada
stavros.tavoularis@uottawa.ca

ABSTRACT

We investigated the influence of coherent structures on the dispersion of a passive scalar by studying instantaneous measurements of a plume of dye released in uniformly sheared flow generated in a water tunnel. Measurements were performed using simultaneous stereo particle image velocimetry and planar laser-induced fluorescence to obtain instantaneous concentration and velocity maps in cross-sections normal to the flow direction. Coherent vortices were observed to effectuate scalar transport by inducing motions which displaced dyed fluid. Dye was observed to preferentially congregate within vortex cores and far away from vortices, whereas regions adjacent to vortices were less likely to contain dye. A conditional eddy analysis demonstrated that counter-rotating vortex pairs associated with hairpin vortices were responsible for both large Reynolds stress events and large scalar flux events. This observation was supported by the fact that the Reynolds stress was found to be correlated with the scalar flux.

Introduction

Coherent structures are the recurring, dominant, vortical, large-scale flow patterns that are ubiquitous in turbulent flows. Previous experimental and numerical studies have shown that hairpin vortices are the predominant coherent structures in turbulent boundary layers (Adrian, 2007; Wu & Moin, 2010) as well as in other shear flows (Vanderwel & Tavoularis, 2011; Ghaemi & Scarano, 2011). The generation of such structures has been explained by the lifting and stretching of quasi-two-dimensional roller vortices. Coherent structures have been shown to be a primary mechanism for the generation of Reynolds stresses that dominate the transport of momentum, so that their control is essential for drag and noise reduction. As a corollary of Reynolds analogy, which connects heat and mass transport to momentum transport, one would expect that coherent structures should also be largely responsible for scalar transport. This connection has been demonstrated qualitatively by flow visualizations of scalar field patterns in turbulent boundary layers (Head & Bandyopadhyay, 1981; Kline *et al.*, 1967; Falco, 1977). More recently, Wu & Moin (2010) also observed hairpin vortices in isocontours of a scalar field examined by direct numerical simulations.

The effects of coherent structures on scalar transport are particularly important in the context of environmental flows. Katul *et al.* (1997) and Li & Bou-Zeid (2011) have noted that, in the atmospheric surface layer, the ejection and sweep motions that are typically associated with coherent structures are responsible for much of the land-surface evaporation, heat and momentum fluxes. Provenzale (1999) reviewed the impact of coherent vortices in quasigeostrophic flows in the ocean and the atmosphere and described how scalars seeded within vortices experience reduced dispersion compared to the free stream, and become, in a sense, islands of stability. Investigations of particle dispersion have also demonstrated that coherent structures are responsible for particle clustering, which has direct ramifications to reactive flows such as combustion as well as to droplet coalescence and the formation of clouds in the atmosphere (Shaw *et al.*, 1998; Rouson & Eaton, 2001). Better understanding of the role of coherent structures in scalar transport is also important for working towards the refinement of turbulent diffusion models to better be able to resolve their effects.

In view of the importance of scalar dispersion in many applications, it is rather surprising that the role coherent structures play on the dispersion of passive scalars has not yet been studied quantitatively and systematically in the laboratory. The goal of the present work is to investigate both qualitatively and quantitatively the influence of coherent structures on turbulent dispersion. We investigated a plume of dye released from a point source in uniformly sheared flow (USF) generated in a water tunnel. This turbulent field is nearly homogeneous but strongly anisotropic, and has a large-scale structure that is dominated by horseshoe/hairpin-shaped vortices (Vanderwel and Tavoularis, 2011), comparable to those found in turbulent boundary layers.

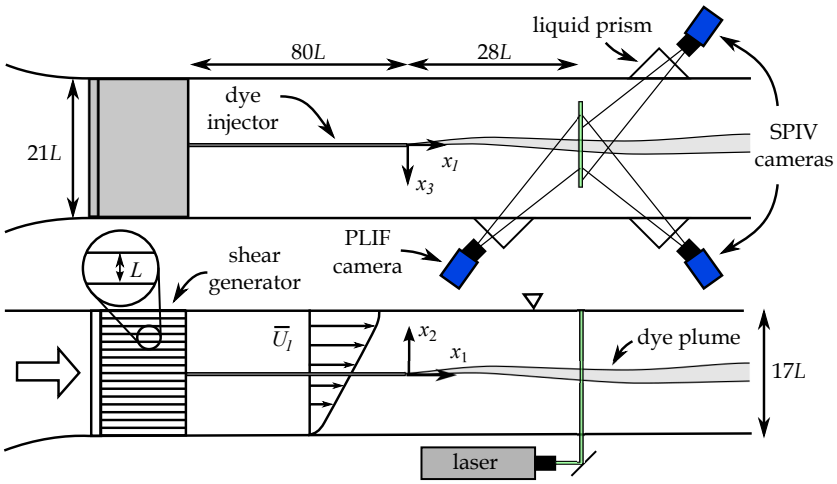

Figure 1: Top and side views of the experimental apparatus and main instrumentation in the water tunnel test section; $L = 25.4$ mm is the spacing of the shear generator.

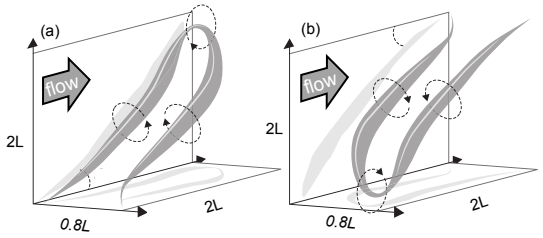

Figure 2: Sketches of (a) an upright and (b) an inverted hairpin vortex (adapted from Vanderwel & Tavoularis, 2011).

Apparatus and Flow Conditions

A sketch of the experimental facility and main instrumentation is presented in figure 1. Uniform shear was generated with the use of a shear generator. The streamwise velocity at the centre of the channel was $U_c = 0.18$ m/s. The turbulence was nearly homogeneous on transverse planes and strongly anisotropic, and had a turbulence Reynolds number $Re_\lambda \approx 150$. The turbulence integral lengthscale, which was comparable to the shear generator spacing $L = 25.4$ mm, was much smaller than the dimensions of the flow domain. The mean and turbulent properties of the flow have been documented in detail by Vanderwel & Tavoularis (2011).

Previous measurements in this flow have documented the prevalence of horseshoe/hairpin-shaped vortices (Vanderwel & Tavoularis, 2011), having similar characteristics to those found in turbulent boundary layers at comparable Re_λ. In USF, both upright and inverted hairpins were observed, with idealised shapes as illustrated in figure 2, whereas, in turbulent boundary layers, the presence of the wall suppresses the development of inverted hairpin vortices. These coherent vortices were distributed evenly throughout the present flow.

Fluorescent dye (Rhodamine 6G) was released isokinetically from a fine tube in the fully developed region of the flow with a source concentration of $C_S = 0.3$ mg/ℓ. Buoyancy effects were negligible and molecular diffusion was extremely weak, as this dye has a Schmidt number of 2500±300.

Simultaneous measurements of the instantaneous concentration and velocity maps were obtained in planes normal to the flow direction. Maps of all three components of the turbulent velocity were obtained via a two-camera stereoscopic particle image velocimetry (SPIV) system (FlowMaster, LaVision). Maps of the concentration were determined using the planar laser-induced fluorescence (PLIF) technique from dye fluorescence maps obtained with a third digital camera (PCO-Edge), synchronized with the SPIV system. Liquid prisms were used to prevent optical aberrations due to horizontal astigmatism associated with the oblique viewing angle into the test section. Details of the measurement procedure and the plume characteristics have been documented elsewhere (Vanderwel & Tavoularis, 2014*a*,*b*,*c*).

Proximity of dyed fluid to coherent structures

As a first step for investigating the connection between the coherent structures and the scalar dispersion, we considered whether the locations of fluid marked by dye were correlated with or otherwise related to the locations of coherent structures. Two representative instantaneous velocity maps are presented in figures 3a,d. An algorithm (Vanderwel & Tavoularis, 2011) applied to these maps identified the cores of coherent vortices as regions of the flow where the swirling strength exceeded 25% of the maximum measured swirling strength; the cross-sectional area of each structure was subsequently determined by an area-growing algorithm as the region around each core in which the swirling strength exceeded 5% of the maximum. It was assumed that the cross-sections of the vortices had elliptical shapes and an ellipse with the minimum area was fit to the boundary of each vortex, as identified previously; then, the vortex centre was defined as the midpoint between the two foci of the ellipse and the vortex diameter was defined as the average of its major and minor axes. This method successfully distinguished neighbouring vortices, and especially vortex pairs, which were separated by regions of negligible swirling strength, corresponding to reversals of vorticity direction. Figures 3b,e indicate the locations of vortices identified by the algorithm in these examples, together with vector maps of the local relative

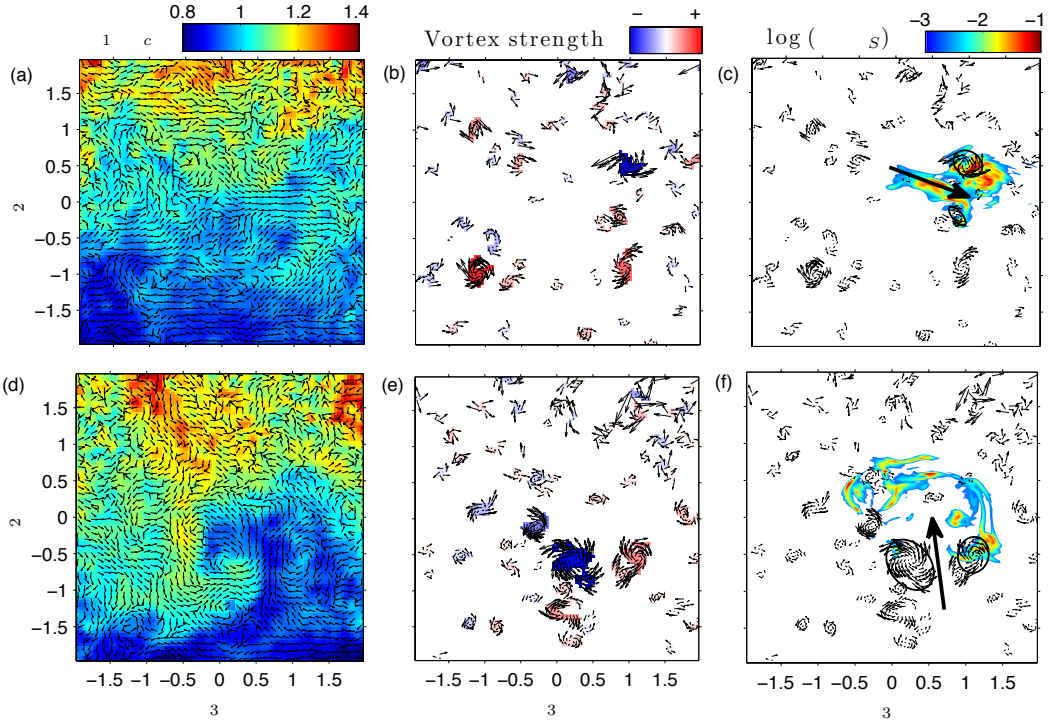

Figure 3: Two representative instantaneous sets of maps (a-c and d-f) illustrating the influence of coherent structures on dye transport. (a,d) transverse velocity vector maps with superimposed coloured contours of the streamwise velocity; (b,e) relative velocity vector maps within vortices, with coloured contours corresponding to vortex strength; (c,f) concentration maps superimposed on relative velocity vector maps within vortices. Pairs of relatively strong counter-rotating vortices, marked by ellipses, are seen to induce flows which displace dyed fluid.

velocities, which illustrate the direction and strength of local rotation. The vortices were roughly evenly distributed throughout the flow, as anticipated in view of the homogeneity of the turbulence. Several pairs of counter-rotating vortices are apparent, which are interpreted as cross-sections of hairpin vortices.

Representative instantaneous concentration maps, measured simultaneously with the corresponding velocity maps, are shown superimposed on the local relative velocity maps in figures 3c,f. Two different aspects of forceful scalar transport enacted by coherent structures can be seen readily in these figures: in figure 3c, a strong vortex pair induces a lateral flow between the two vortices, which transports dye between the pair and away from the plume centreline; in figure 3f, a similar vortex pair, presumably the cross-section of an upright hairpin vortex, induces an upward flow of undyed fluid, which in turn displaces dyed fluid further upwards. These examples clearly demonstrate an important point, namely that the fact that the locations of dye and coherent structures do not necessarily coincide does not mean that dye transport and dispersion are not connected intimately to coherent structure actions. This conjecture was supported by statistical analysis, which found no significant cross-correlation between concentration and vortex locations. Our investigation has demonstrated that the relationship between dyed fluid regions and coherent structures depends on their initial relative positions: if dyed fluid happens to be near the base of a vortex pair, it would be transported between the pair, but, if the dyed fluid happens to be initially on the other side of the pair, it would

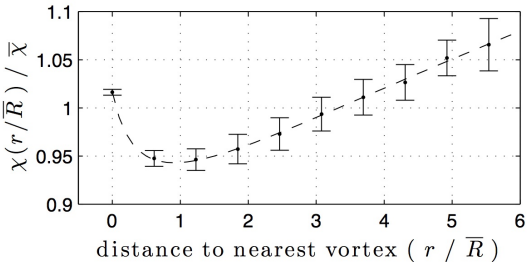

Figure 4: Variation of the normalized average local volume fraction of dye with normalized distance from the nearest vortex centre; uncertainty bars indicate the standard deviations of measurements at streamwise positions having $x_1/L = 20$, 28, and 35.

be pushed further away from it. In either case, the coherent structure would make a major impact on scalar transport.

To further investigate any possible relationship between the locations of regions containing dyed fluid and the locations of coherent structures, we calculated the average local volume fraction $\chi(r)$ of dyed fluid, as a function of distance r from the nearest vortex centre. This property is deemed to indicate the likelihood of dye presence at the given distance. To calculate $\chi(r)$, we first identified the vortex that was nearest to each pixel in the measurement domain and then determined the distance between the pixel and the vortex centre. Finally, we computed the volume fraction as the ratio of the number of pixels with non-zero

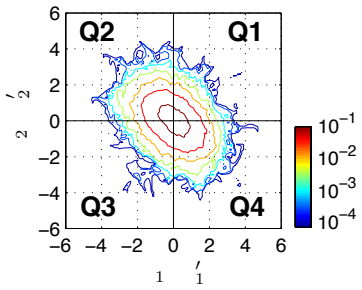

Figure 5: Contours of the joint pdf of u_1 and u_2 illustrating the predominance of Reynolds stress events to the Q2 and Q4 quadrants; primes indicate standard deviations.

concentration and the total number of pixels in annular regions with mean radius equal to r. We normalized r by the mean vortex radius $\overline{R} = 0.07L$ and $\chi(r/\overline{R})$ by the overall volume fraction $\overline{\chi}$ in the entire measurement domain. The corresponding results are presented in figure 4. The likelihood of dye presence has a minimum near the periphery of the vortex; this indicates that there is some segregation of dye in the core of the vortex and a tendency for out-of-core dye to stay away from the core. The fact that the likelihood of dye presence in the vortex core is only slightly higher than elsewhere in the flow explains the observed lack of significant correlation between dye concentration and vortex location. The trend of dye volume fraction can be explained by the following conjecture: dye that was injected into the vortex core generally stayed in the core, whereas dye that was injected outside the core could be wrapped around it or pushed away by transverse motions induced by a vortex pair, without penetrating the vortex core. Lastly, dye appears to be segregated preferentially far away from vortices. We may speculate that these are regions with nearly uniform momentum, which appear between hairpin vortices in the flow (Vanderwel & Tavoularis, 2011).

Conditional eddy analysis

In order to further investigate the influence of coherent structures on scalar transport, we applied a conditional eddy analysis, which is a method capable of reconstructing representative instantaneous flow patterns associated with the occurrence of significant flow events. The conditional eddy approach has been used by previous authors (Adrian & Moin, 1988; Adrian, 2007) to identify large-scale coherent structures in the turbulent boundary layer, as patterns that occurred when the nearby flow field met the condition of a large Reynolds stress in the Q2 quadrant ($u_1 < 0$ and $u_2 > 0$); reconstruction of the mean flow field resulted in a pattern that had the shape of a typical hairpin vortex.

In the present work, we first adapted conditional eddy analysis for vortex identification in USF and then extended it, for the first time, for identification of scalar transport events. As in turbulent boundary layers, in USF, the Reynolds stress tensor is anisotropic and the joint pdf of the streamwise and transverse velocity fluctuations (see figure 5) indicates a proclivity for events in the Q2 ($u_1 < 0$ and $u_2 > 0$) and Q4 ($u_1 > 0$ and $u_2 < 0$) quadrants, which is consistent with the negative correlation between u_1 and u_2. It is noted that, unlike turbulent boundary layers in which a one-sided orientation of hairpin vortices is imposed by the wall, USF has hairpins in both "upright" and "inverted"

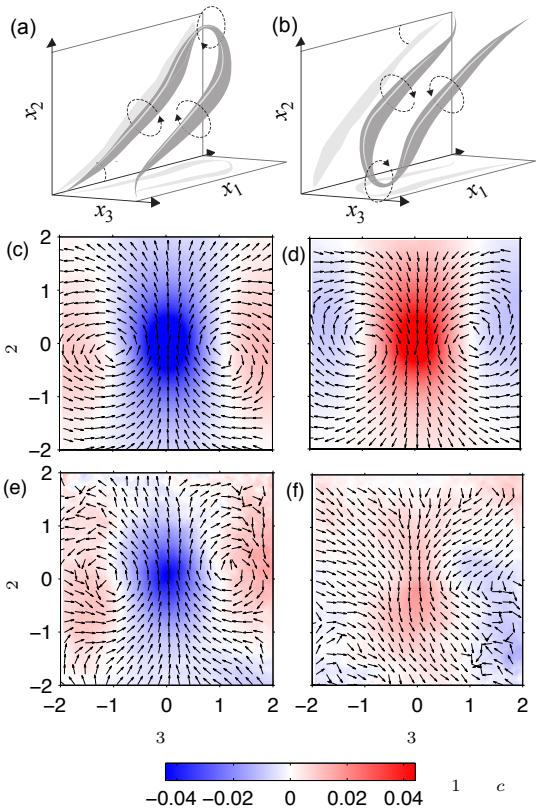

Figure 6: Conditionally averaged flow fields based on (c) large Reynolds stress events in Q2 and (d) in Q4 and (e) large scalar flux events having large positive values of cu_2 and (f) large negative values of cu_2, which indicate counter-rotating vortex pairs corresponding with the cross-sections of (a) upright and (b) inverted hairpin vortices.

orientations (Vanderwel & Tavoularis, 2011). For this reason, we identified large Reynolds stress events in both the Q2 and the Q4 quadrants as those that met the condition $|u_1 u_2| > 4u_1' u_2'$ (Antonia, 1981). Unlike previous studies which utilized a Linear Stochastic Estimation (LSE) to approximate the conditional flow field (Adrian, 1994), we determined the conditional flow field directly from the ensemble-average of the shifted instantaneous flow fields; reanalyzing the results using LSE yielded equivalent results without significant improvement. The corresponding mean flow fields in planes normal to the flow are shown in figures 6a,b. Both flow fields are cross-sections of pairs of counter-rotating vortices with sizes comparable to the characteristic lengthscale L and consistent with the signatures of a hairpin vortex. Q2 events correspond to upright hairpin vortices (figure 6e), whereas Q4 events correspond to inverted hairpin vortices (figure 6f).

Subsequently, we determined the conditional eddies that met the scalar flux condition $|cu_2| > 4c'u_2'$, where c is the dye concentration fluctuation. The resulting flow field associated with large positive cu_2 events (figure 6c) clearly indicates a pair of counter-rotating vortices corresponding to an upright hairpin vortex, which is also associated with large Reynolds stress events in the Q2 quadrant. The flow field associated with large negative cu_2 events (figure 6d) is consistent with the presence of inverted hairpin vortices, which are also associated with large Reynolds stress events

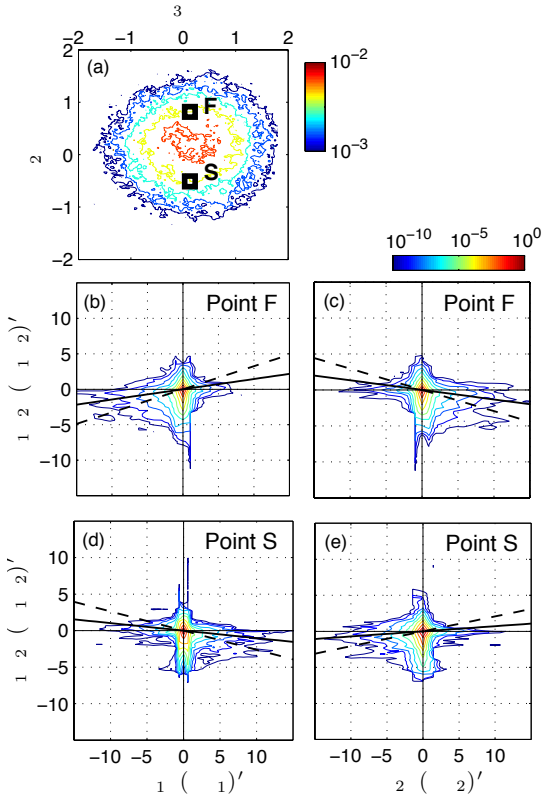

Figure 7: (a) Map of the mean concentration $\overline{C}/C_S$ with two regions of interest indicated by squares; (b-d) joint pdfs of the streamwise cu_1 and transverse cu_2 scalar fluxes and the Reynolds stress u_1u_2, measured at points F and S and normalized by the corresponding standard deviations; the solid line indicates the correlation coefficient whereas the dashed line indicates the correlation coefficient determined from values conditioned on $C > 0$.

in the Q4 quadrant. The conditional eddies identified by the large scalar flux condition appear to be less distinct than those identified by the large Reynolds stress condition, because scalar flux events were restricted only within the present slender plume, whereas Reynolds stress events occurred in the entire flow domain. The results of this conditional eddy analysis clearly demonstrate that coherent vortices are a dominant mechanism for turbulent scalar transport.

In support of the previous assertion, we investigated the possible correlation between the Reynolds stress and the scalar flux. Such a correlation was also observed by Li & Bou-Zeid (2011), who studied the turbulent transport of heat and water vapour in the atmospheric surface layer. We present representative measurements at two locations on either side of the axis of the plume, along the mean velocity gradient direction, near the two inflection points of the mean concentration profile (points F and S, respectively, as indicated in figure 7a). The joint pdfs of the scalar fluxes and the Reynolds stress are presented in figure 7b-e. At point F, the joint pdf of cu_1 and u_1u_2 is clearly biased to the third quadrant, indicating a positive correlation between the Reynolds stress and the streamwise scalar flux. The joint pdf of cu_2 and u_1u_2 is clearly biased to the fourth quadrant, indicating a negative correlation. Similarly at point S, the

Point	Scalar flux	ρ	$\rho\|(C>0)$
F	cu_1	+0.14	+0.33
F	cu_2	-0.13	-0.30
S	cu_1	-0.10	-0.26
S	cu_2	+0.07	+0.21

Table 1: Values of the correlation coefficient between the scalar flux components and the Reynolds stress and the same correlation coefficient determined from values conditioned on $C > 0$.

joint pdf of cu_1 and u_1u_2 is biased to the fourth quadrant, indicating a negative correlation, whereas the joint pdf of cu_2 and u_1u_2 is biased to the third quadrant, indicating a positive correlation. The change of sign of the correlations at points F and S is consistent with the change of sign of the mean scalar fluxes at these points. The fact that the correlations involving cu_1 and cu_2 have opposite signs is consistent with the fact that the streamwise and transverse scalar fluxes are negatively correlated at these locations (Vanderwel & Tavoularis, 2014*a*). The values of the correlation coefficients are presented in table 1 and are also indicated by lines in figure 7. The magnitudes of correlation coefficients were fairly low due to the fact that the present plume was particularly slender and the scalar signal was highly intermittent; therefore, correlation coefficients were also determined considering only values conditioned on dye being present ($C > 0$). The resulting conditional correlation coefficients were significantly larger in magnitude than the unconditional ones, which further supports the conjecture that coherent structures simultaneously transport both mass and momentum.

Conclusions

The influence of coherent structures on turbulent dispersion of passive scalars was qualitatively and quantitatively investigated from simultaneous measurements of the instantaneous concentration and velocity fields in a dye-marked plume. Despite the absence of a direct correlation between the scalar concentration and the locations of coherent structures, dye was found to segregate preferentially within vortex cores and away from vortices and less likely to be present in the periphery of vortices. A conditional eddy approach was applied to the study of scalar flux and the correlation between the Reynolds stress and the scalar flux was documented. These results demonstrate that coherent structures are the main cause of large scalar flux events and play a dominant role in turbulent diffusion.

Financial support by the Natural Sciences and Engineering Research Council of Canada (NSERC) is gratefully acknowledged.

REFERENCES

Adrian, R.J. 1994 Stochastic estimation of conditional structure: a review. *Appl. Sci. Res.* **53** (3-4), 291–303.

Adrian, R.J. 2007 Hairpin vortex organization in wall turbulence. *Phys. Fluids* **19** (4), 041301.

Adrian, R.J. & Moin, P. 1988 Stochastic estimation of organised turbulent structure: homogeneous shear flow. *J. Fluid Mech.* **190**, 531–559.

Antonia, R.A. 1981 Conditional sampling in turbulence measurement. *Annu. Rev. Fluid Mech.* **13** (1), 131–156.

Falco, R.E. 1977 Coherent motions in outer region of turbulent boundary layers. *Phys. Fluids* **20** (124).

Ghaemi, S. & Scarano, F. 2011 Counter-hairpin vortices in the turbulent wake of a sharp trailing edge. *J. Fluid Mech.* **689**, 317–356.

Head, M.R. & Bandyopadhyay, P. 1981 New aspects of turbulent boundary-layer structure. *J. Fluid Mech.* **107**, 297–338.

Katul, G., Kuhn, G., Schieldge, J. & Hsieh, C.-I. 1997 The ejection-sweep character of scalar fluxes in the unstable surface layer. *Bound.-Lay. Meteorol.* **83** (1), 1–26.

Kline, S.J., Reynolds, W.C., Schraub, F.A. & Runstadler, P.W. 1967 The structure of turbulent boundary layers. *J. Fluid Mech.* **30** (04), 741–773.

Li, D. & Bou-Zeid, E. 2011 Coherent structures and the dissimilarity of turbulent transport of momentum and scalars in the unstable atmospheric surface layer. *Bound.-Lay. Meteorol.* **140** (2), 243–262.

Provenzale, A. 1999 Transport by coherent barotropic vortices. *Annu. Rev. Fluid Mech.* **31** (1), 55–93.

Rouson, D.W.I. & Eaton, J.K. 2001 On the preferential concentration of solid particles in turbulent channel flow. *J. Fluid Mech.* **428**, 149–169.

Shaw, R.A., Reade, W.C., Collins, L.R. & Verlinde, J. 1998 Preferential concentration of cloud droplets by turbulence: Effects on the early evolution of cumulus cloud droplet spectra. *J. Atmos. Sci.* **55** (11), 1965–1976.

Vanderwel, C. & Tavoularis, S. 2011 Coherent structures in uniformly sheared turbulent flow. *J. Fluid Mech.* **689**, 434–464.

Vanderwel, C. & Tavoularis, S. 2014*a* Measurements of turbulent diffusion in uniformly sheared flow. *J. Fluid Mech.* **754**, 488–514.

Vanderwel, C. & Tavoularis, S. 2014*b* On the accuracy of PLIF measurements in slender plumes. *Exp. Fluids* **55** (1801).

Vanderwel, C. & Tavoularis, S. 2014*c* Relative dispersion of a passive scalar plume in turbulent shear flow. *Phys. Rev. E* **89** (4), 041005.

Wu, X. & Moin, P. 2010 Transitional and turbulent boundary layer with heat transfer. *Phys. Fluids* **22** (8), 085105.